JOURNAL OF GEOPHYSICAL RESEARCH, VOL. 112, D23104, doi:10.1029/2007JD008945, 2007

Insights into Tropical Tropopause Layer processes using global models

A. Gettelman[1] and T. Birner[2]

Received 10 May 2007; revised 8 August 2007; accepted 21 August 2007; published 11 December 2007.

[1] The climatology of the Tropical Tropopause Layer (TTL) in two state-of-the-art general circulation models is compared with observations. Results indicate that global models are able to resolve key features of the TTL, including the mean state and the variability of temperature, ozone, clouds, and thermal structure. The agreement indicates that large-scale processes, and the large-scale effects of small-scale processes, such as convection, are likely the dominant contributors to the observed climatological structure of the TTL and to the observed annual cycle and variability at scales larger than several hundred kilometers. Cloud processes are still uncertain due to their heavily parameterized treatment in models, and limited observations of clouds in the TTL. The bulk treatment of clouds appears sufficient to properly resolve the large-scale structure of the TTL.

Citation: Gettelman, A., and T. Birner (2007), Insights into Tropical Tropopause Layer processes using global models, *J. Geophys. Res.*, *112*, D23104, doi:10.1029/2007JD008945.

1. Introduction

[2] The Tropical Tropopause Layer (TTL), the region in the tropics within which air has characteristics of both the troposphere and the stratosphere, is a critical region of the atmosphere. The concept that the tropical tropopause is not a material surface is not particularly new [*Atticks and Robinson*, 1983], but the concept has gained much attention recently. The TTL has been analyzed recently by (among others) *Highwood and Hoskins* [1998], *Folkins et al.* [1999], and *Gettelman and Forster* [2002].

[3] The TTL is the source region for most air entering the stratosphere, and the chemical boundary conditions of the stratosphere are set in the TTL. Clouds in the TTL, both thin cirrus clouds and convective anvils, have a significant impact on the radiation balance and hence tropospheric climate [*Stephens*, 2005]. Studies by *Gettelman et al.* [2002a], *Fueglistaler and Haynes* [2005], and *Randel et al.* [2001] have shown that the large-scale structure of the TTL sets the water vapor distribution and that details of convective processes are not important. However, *Sherwood et al.* [2003] have argued that convective overshooting and irreversible mass transport is important. Recent cloud-resolving modeling studies [*Küpper et al.*, 2004; *Kuang and Bretherton*, 2004; *Robinson and Sherwood*, 2006] yielded different conclusions as to the role of small-scale convective overshoots in the heat and moisture budgets of the TTL. The reasons for this discrepancy are currently not well understood.

[4] In this work we will present a climatology of the TTL from two global models, and compare it to recent observations of the TTL. We seek to investigate whether models can reproduce key structural features of the TTL and their variability in space and time. We also seek to investigate interrelationships between the thermal structure and trace species such as ozone and water vapor. We hypothesize that the comparison between sparse observations and sets of fields from simulations at various time and space resolutions will enable us to make conclusions about what processes are important in the TTL.

[5] Our hypothesis is that the TTL exists because of the combination of several basic processes which are well described by global models with horizontal resolutions on the order of 100 km and vertical resolutions of the order of a kilometer. Radiation is perhaps the most critical process in the TTL [*Gettelman et al.*, 2004]. Radiative contributions from carbon dioxide in the TTL [*Thuburn and Craig*, 2002] and ozone near the cold point [*Randel et al.*, 2006] are crucial. In addition, convective heating [*Gettelman et al.*, 2001, 2004] and forcing by large-scale waves, both locally [*Fujiwara and Takahashi*, 2001] and nonlocally, by the stratospheric overturning (Brewer-Dobson) circulation [*Brewer*, 1949; *Holton et al.*, 1995] are important for the variability of the TTL. However, there are other processes such as convective mass transport [*Sherwood et al.*, 2003] and small-scale waves [*Potter and Holton*, 1995] which are not well reproduced by large-scale models. If unresolved and parameterized processes are important, it is unlikely that models will get key relationships in the TTL correct. The relative importance of these processes is still uncertain (as noted above).

[6] To define the TTL we focus on the vertical structure, and we adopt the definition of *Gettelman and Forster* [2002] as the layer between the level of maximum convective outflow and the cold point tropopause, where the maximum

[1] Atmospheric Chemistry Division, National Center for Atmospheric Research, Boulder, Colorado, USA.
[2] Department of Physics, University of Toronto, Toronto, Ontario, Canada.

0148-0227/07/2007JD008945$09.00

convective outflow level is diagnosed from the minimum potential temperature lapse rate. This definition is not the only possible one, but conceptually marks the boundary between which air is generally tropospheric (below) and stratospheric (above). The definition is convenient because the TTL can be diagnosed locally from a temperature sounding, and facilitates comparisons with observations.

[7] Below we briefly describe the methodology for diagnosing aspects of the TTL, as well as observations and models we are using (section 2). We then present a climatology of the TTL from two models (section 3). In section 3 we also present a limited set of observations, and refer to previous work which describes in more detail the observed climatology of the TTL. In the discussion (section 4) we will summarize the results and conclude (section 5) by relating results to key processes in the TTL.

2. Methodology

[8] We will focus on several convenient diagnostics for different aspects of the TTL. The motivations for diagnostics, their observed climatology and trends are detailed by *Gettelman and Forster* [2002], and we discuss them only briefly here.

[9] The base of the TTL is diagnosed as the level of maximum impact of convection on the thermal structure. Convection follows a moist adiabat which tends toward the dry adiabatic lapse rate ($dT/dz = -9.8°C\ km^{-1}$) in the upper troposphere as water vapor decreases with height. As convection diminishes, this profile will begin to relax toward the radiative equilibrium of the stratosphere, and the magnitude of the lapse rate will decrease. The lapse rate of potential temperature is zero for a dry adiabat, and so the minimum magnitude of the potential temperature lapse rate is the level of maximum impact of convection. Because we are using potential temperature we will adopt the convention that the lapse rate (Γ_θ) is $\Gamma_\theta = d\theta/dz$. Γ_θ is positive because potential temperature increases with height, thus we are interested in the minimum. *Gettelman and Forster* [2002] also noted that the lapse rate minimum (or LRM) level often coincides with the minimum ozone mixing ratio, which is indicative of a maximum outflow of near surface air with low ozone mixing ratios [*Folkins et al.*, 2002]. We will also examine the climatology of the minimum ozone (O3min) pressure and the value of ozone at this level.

[10] Another important level in the TTL is the Level of Zero radiative Heating (LZH). This usually lies around 15 km or 150 hPa [*Gettelman et al.*, 2004]. Above this level, in clear sky, air will tend to rise into the stratosphere, and below this it will sink. The shape of the radiative heating rate profile and the LZH location are a consequence of relaxation due to dynamic forcing. The radiative relaxation is determined by: the temperature profile, the absorption of radiation due to the increase of ozone with height, the presence of carbon dioxide heating and the decrease in radiative cooling due to water vapor absorption as water vapor concentrations are limited by cold temperatures. As noted by *Gettelman et al.* [2004] and *Corti et al.* [2006], among others, the LZH can change locally by several kilometers depending on the distribution of clouds in the TTL and below.

[11] Finally, we diagnose the "top" of the TTL by looking at the cold point tropopause (CPT or just Cold Point-CP). The CPT is a useful diagnostic, because water vapor in the stratosphere is controlled broadly by its temperature [*Brewer*, 1949], though there may be important local processes in convective or cirrus clouds which modify the quantitative value of water vapor. While there is some air above the CPT which may have tropospheric characteristics and there is some convection above the CPT [*Gettelman et al.*, 2002b; *Liu and Zipser*, 2005; *Dessler et al.*, 2006], air is basically stratospheric above this level.

[12] We will use observations described below to help diagnose these levels, and we will refer extensively to previously published observations and analyses noted above. Because we are looking in the deep tropics and focusing on processes, we will focus in this analysis on the vertical and zonal structure of the TTL within the tropical confines of the overturning Hadley-Walker circulation, and not discuss the meridional boundaries of the TTL.

[13] Below we describe the observations and the two major models we will be using for this study. We will examine several different versions of the models to attempt to understand the effects of (1) different model physics, (2) averaging at different temporal scales: Instantaneous, Daily and Monthly, (3) vertical resolution and (4) including active chemistry in the TTL.

2.1. Observations

[14] To better characterize the TTL, we will show a limited set of recent observations. Following the diagnostics described above we will use observations of temperatures and ozone concentration. For both ozone and temperature we will use the Southern Hemisphere Additional Ozonesonde (SHADOZ) network of stations [*Thompson et al.*, 2003]. Profiles are recorded since 1998 roughly once a week for most stations. We analyze 10 stations between 20S and 20N for the period 1998–2006. Stations used are shown in Figure 5e. Additionally, we use 12-hourly temperature profiles from operational radiosonde stations between 20S and 20N from the U.S. station network (referred to as RAOB below) for the years 1998–2005. The RAOB data are available from the Stratospheric Processes and their Role in Climate (SPARC) data center (http://www.sparc.sunysb.edu). All sonde data used in this study have high-vertical resolution (~50 m or better) and there are 21 stations in total.

[15] In addition, we will examine temperature records from Global Positioning System (GPS) radio occultation soundings. These provide accurate temperature profiles at 200m vertical resolution along a 200 km horizontal path. GPS sensing of the TTL is described by *Randel and Wu* [2005]. We will use GPS temperatures from the German CHAMP satellite, described by *Wickert et al.* [2001] and *Hajj et al.* [2004].

[16] In addition to these observations, we will cite previous work on observations of the TTL where appropriate. These come from a wide array of data sources looking at the thermal and chemical structure, the distribution of clouds, and radiative and trajectory models.

2.2. Models

[17] Output from two state-of-the-art coupled chemistry climate models is used: the Whole Atmosphere Community Climate Model, Version 3 (WACCM) and the Canadian

Middle Atmosphere Model (CMAM). Both models perform well relative to observations and to other coupled models [*Eyring et al.*, 2006]. Simulations are coupled in the sense that variations in radiatively active species like water vapor and ozone affect model heating rates. The models have different transport and advection schemes. Clouds are represented differently except for the use of different versions of the same deep convective parameterization [*Zhang and McFarlane*, 1995]. Three years of output with a repeating annual cycle of surface forcing are analyzed for each model, after allowing for spin up and equilibration. For the TTL this is sufficient to capture most interannual variability (which is NOT true for high latitudes, or the impact of high latitudes on the tropics). The simulations are run with climatological SSTs, so there is no effect of the El-Niño Southern Oscillation. None of the models used in this study generates an internal Quasi Biennial Oscillation. The runs are sufficient to capture a climatology, and do not differ strongly from longer runs such as those discussed by *Eyring et al.* [2006].

2.2.1. WACCM

[18] WACCM, from the National Center for Atmospheric Research (NCAR) spans the atmosphere from the surface to the lower thermosphere and is described by *Garcia et al.* [2007]. It is based on the framework of the Community Atmosphere Model, version 3 (CAM), a General Circulation Model (GCM) described by *Collins et al.* [2006]. WACCM uses CAM as its base, and adds parameterizations for chemistry and upper atmospheric processes. The CAM top is 2 hPa (45 km), while the WACCM top is 5×10^{-6} hPa (140 km). CAM does not fully resolve the dynamics of the stratosphere. The chemistry module for WACCM and CAM is derived from the three dimensional chemical transport Model for Ozone and Related chemical Tracers (MOZART) [*Brasseur et al.*, 1998; *Horowitz et al.*, 2003; *Kinnison et al.*, 2007].

[19] In this study we use WACCM at two different vertical resolutions, and a CAM simulation. The standard case (WACCM-L66) has 66 levels in the vertical with ~1 km vertical resolution in the TTL. We also use a version of WACCM with ~0.3 km resolution from 5–20 km for a total of 103 levels (WACCM-L103). The high resolution grid midpoints are shown as tick marks on Figure 10. In addition, we use a version of CAM which includes more sophisticated tropospheric chemistry (which adds hydrocarbon chemistry and short lived species to the stratospheric chemistry in WACCM) and has 26 vertical levels, with vertical resolution of ~1 km in the TTL. Horizontal resolution of the WACCM simulations is $4^\circ \times 5^\circ$, and $2^\circ \times 2.5^\circ$ for CAM.

2.2.2. CMAM

[20] CMAM spans the atmosphere from the surface to the upper mesosphere/lower thermosphere and its general features are described by *Beagley et al.* [1997] and *de Grandpré et al.* [1997, 2000]. It is based on the Canadian Centre for Climate Modeling and Analysis (CCCma) third-generation atmospheric general circulation model [*Scinocca and McFarlane*, 2004]. In standard setup CMAM does not include tropospheric chemistry (with no chemistry on model levels below about 400 hPa). Here a version of CMAM that performs chemistry calculations on all levels is used (courtesy of David Plummer). The chemical mechanism has not changed from that used in the standard CMAM and is equivalent to methane-NOx chemistry for the troposphere. Notable changes from the standard CMAM include the addition of surface emissions of NOx and CO, modified photolysis rates to account for cloud effects and a more robust representation of wet and dry deposition. Lightning produced NOx (an important source of tropospheric ozone, particularly in the tropics) has not been included, i.e., tropospheric ozone is expected to be biased low. Dynamics and chemical transport in CMAM are calculated using a T47 spectral representation. Vertically the model has 71 layers, extending to around 100 km altitude. The vertical resolution in the TTL is ~1 km, i.e., very similar to that in WACCM-L66.

3. Results

[21] To present a basic climatology we first discuss the basic TTL structure from observations and models, the thermal structure and the mean structure of the TTL. We then examine the variability of the TTL, seasonal contrasts for January and July, and finally focus on clouds in the TTL. We have examined all diagnostics for all models, and where only one model is shown, the others show similar results.

3.1. Basic TTL Structure

[22] Figure 1 shows the Cold Point Tropopause (CPT) temperature (Figure 1a) and Minimum Lapse Rate (LRM) pressure (Figure 1b) for January from GPS observations and WACCM from 20S–20N latitude. This represents the "top" and "bottom" of the TTL respectively. The GPS data represents approximately 700 profiles in the tropics in the month of January 2006. Figure 1 illustrates the high frequency variability of the TTL from both WACCM (L103) and GPS observations. The mean and range of CPT temperatures produced by the model, including the zonal variability, are similar to observations. The standard deviation (σ) of GPS observed CPT is ~3.9 K, while for WACCM it is ~3.4 K, i.e., WACCM slightly underestimates variability, although the difference might also be due to GPS sampling or horizontal resolution (which at ~200 km is finer than WACCM).

[23] The Lapse Rate Minimum (LRM) pressure (Figure 1b) also has large variability. In general it is located around 200–250 hPa (10–12 km), and is at higher altitude in regions of active convection, and at lower altitude when convection is less active [*Gettelman and Forster*, 2002]. The LRM height is highest (lowest pressure) over the western Pacific and lowest (highest pressure) over the tropical eastern Pacific and Atlantic. WACCM simulations also produce this wide spread, zonal variation and have a similar mean. The variation of GPS observed minimum lapse rate pressure (height) is large with 1σ values of 70 hPa (1.9 km). WACCM has similar LRM pressure variability (1σ = 69 hPa).

[24] The vertical structure of ozone in the TTL is illustrated from SHADOZ observations and several model integrations in Figure 2. SHADOZ observations are from 10 stations located throughout the tropics. Ozone values are higher in July than in January near the tropopause at 100 hPa [*Folkins et al.*, 2006]. The ozone minimum is not well defined but in January it lies at 250–200 hPa (10–11.5 km). This altitude is similar to the LRM height in Figure 1b. Figure 2 also plots

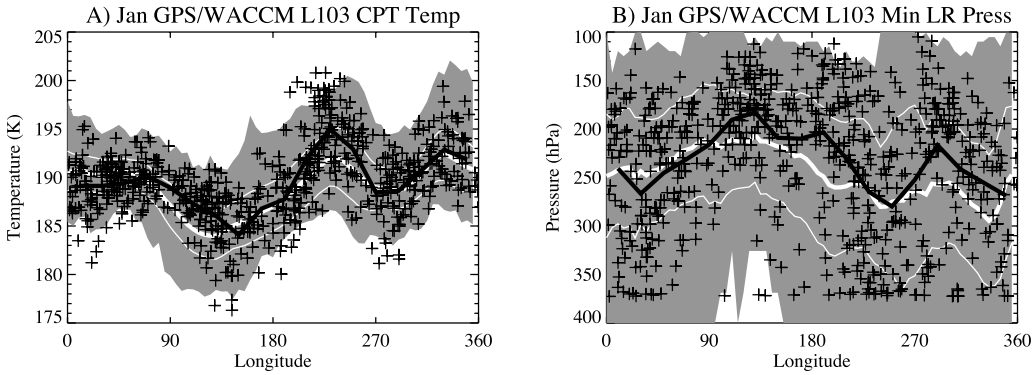

Figure 1. January mean (a) Cold Point Tropopause (CPT) temperatures and (b) Minimum Lapse Rate Pressure from WACCM (gray) and CHAMP GPS observations (black) averaged over the tropics (20S–20N). Gray shaded region is the range of WACCM output, thick white line is the mean, and thin white lines are ±1 standard deviation (σ). GPS observations are marked by black crosses for individual soundings and by a thick black line for the mean.

model simulations, from CMAM (dashed), WACCM (thin dotted) and CAM (thick dotted). There is little difference between sampling the models at SHADOZ station locations (black) or all points (gray), indicating that SHADOZ ozone is representative of the TTL (at least in the simulations). Also plotted are the level of the Cold Point (CP) tropopause, the level of zero heating (LZH), minimum ozone level ($minO_3$) and lapse rate minimum (LRM) level from CMAM, with their 1 σ variability.

[25] The ozone minimum has large variability (partially because it is not well defined). All models are able to simulate the ozone gradients fairly well despite several shortcomings. No attempt has been made to unify the boundary conditions or initialization of the simulations. CMAM has an overall low ozone bias most likely due to missing NOx emissions from lightning. CAM does perhaps the best job of simulating ozone, and is perhaps even a bit high. This is to be expected as CAM has a better description of tropospheric ozone chemistry, and more precursor emissions in the troposphere to produce ozone (note the high January boundary layer ozone in CAM). There are also differences in the simulation of the ozone gradient within the TTL (200–100 hPa), which is likely related to the treatment of convective transport (see discussion of clouds below).

[26] Figure 3 illustrates the potential temperature (θ) lapse rate. The minimum in this quantity represents the level of main convective outflow, approximately the bottom of the TTL. The minimum is better defined in July than January (Figure 3) in both the models and observations. Both CMAM and WACCM properly represent the lapse rate profile, with a minimum at about 200–250 hPa consistent with Figure 1b, although lapse rate values around the minimum are somewhat too high for CMAM and somewhat

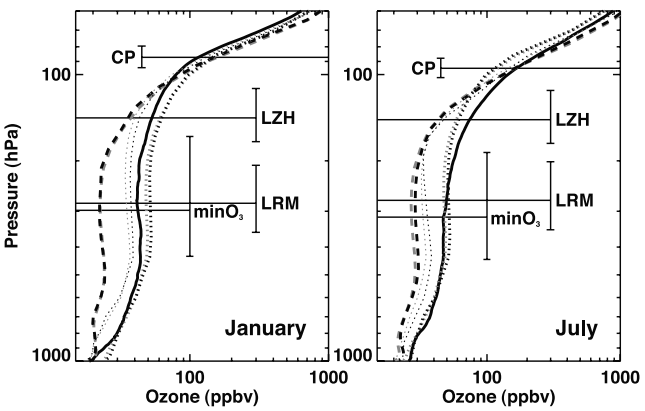

Figure 2. TTL (20S–20N) Ozone profiles for (left) January and (right) July. Shown are SHADOZ ozonesondes (solid black line). CAM, thick dotted; WACCM (66 levels), thin dotted; CMAM, dashed. Black lines are models sampled at SHADOZ station locations; gray lines are model domain averages. Solid lines indicate the Cold Point (CP), Level of Zero Heating (LZH), minimum ozone level (minO3), and minimum lapse rate level (LRM) from CMAM. Error bars indicate 1 standard deviation.

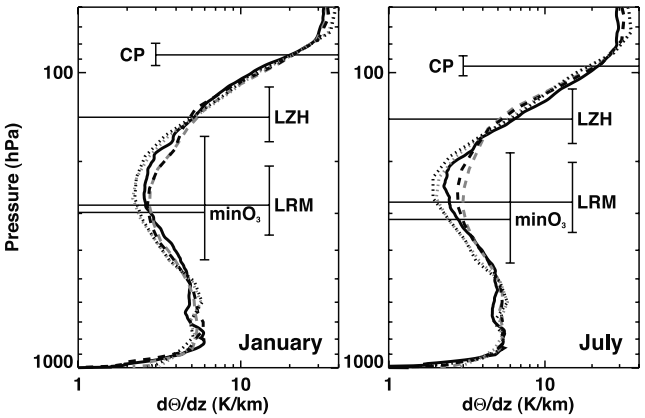

Figure 3. TTL (20S–20N) potential temperature (Θ) lapse rate profiles for (left) January and (right) July. Shown are SHADOZ ozonesondes (solid black line). WACCM (66 levels), thick dotted; CMAM, dashed. Black lines are models sampled at SHADOZ station locations; gray lines are model domain averages. Solid lines indicate the Cold Point (CP), Level of Zero Heating (LZH), minimum ozone level (minO3), and minimum lapse rate level (LRM) from CMAM. Error bars indicate 1 standard deviation.

Table 1. Mean Characteristics of the TTL for January, 20S–20N[a]

Model/Obs	CPT, K	CPT, hPa	LZH, hPa	LRM, hPa	$MinO_3$, hPa	$MinO_3$, ppbv
GPS	189.5	86		234		
RAOB/SHADOZ	189.1	85		257	260	30
WACCM L103 monthly	189.4	88	141	280	269	30
WACCM L103 daily	189.2	89	137	256	229	29
WACCM L103 instant	188.9	88		246	232	28
WACCM L66 monthly	189.1	87	154	265	353	31
CMAM instant	191.2	89	142	270	233	17
CAM L26	190.9	87	158	244	406	42

[a]Cold Point Tropopause (CPT) temperature and pressure, Level of Zero Heating (LZH) pressure, Minimum Lapse Rate (LRM) pressure, and minimum ozone ($MinO_3$) temperature and pressure from indicated sources.

too low for WACCM. The LRM is similar in altitude to the minimum ozone level, consistent with the fact that convective outflow sets both of these levels. The difference between the LRM and minimum ozone level is not significant given the large variability of each level. The CAM lapse rate profile (not shown) degrades near the tropical tropopause due to coarse vertical resolution. WACCM and CMAM both seem to have a more gradual gradient change just above the tropopause than the observations.

[27] The $d\theta/dz$ profile in Figure 3 is related to the stability (N^2) as $N^2 = g/\theta\ (d\theta/dz)$. In both models, the change in gradient above the cold point tropopause is not as sharp as in observations, which leads to a sharp stability spike near the tropopause in observations, which *Birner* [2006] noted in high resolution radiosonde data in the extra-tropics and is also present in the tropics [*Birner et al.*, 2006; S. W. Bell and M. A. Geller, Latitudinal variations in Birner's extra-tropical transition layer, submitted to *Journal of Geophysical Research*, 2007]. In the profile of $d\theta/dz$ this spike is the sudden change to a constant gradient with height at ~80 hPa in Figure 3. However, the models do produce a peak in stability above the tropopause, which is qualitatively similar to observations. The higher vertical resolution model (not shown) does a slightly better job of actually producing a definite maximum in stability above the tropopause than a coarser resolution model.

[28] Table 1 illustrates the tropical average (±20 lat) for these various levels for January from both the GPS and RAOB/SHADOZ observations, as well as from the various simulations. To test sensitivity, analysis has been performed using instantaneous model output (instant) as well as daily and monthly averages. The models may compare better with observations if sampled at station locations (e.g., CMAM CPT in Figure 6a).

[29] The simulations are all able to reproduce the correct TTL structure (also illustrated in the figures): the CPT is close to the right pressure (~85 hPa), the LZH is located below the CPT in the TTL (~150 hPa), and the LRM and O3min levels are comparable (~250 hPa), with the minimum ozone level slightly lower (higher pressure). The minimum average Ozone value is also close to observations (20–40 ppbv). The January tropopause temperature is slightly warmer in CMAM than observed by GPS or simulated by WACCM. The level of zero heating cannot be directly calculated from observations, but has been reported to be close to 150 hPa [*Gettelman et al.*, 2004], similar to the simulated LZH. The lapse rate minimum (LRM) varies tremendously as noted in Figure 1b. The ozone maximum value is higher in CAM, which has tropospheric chemistry. The use of coarser vertical resolution and averaging over a month does not seem to degrade the mean structure of the TTL. We have also examined variability (see below) and found that it also does not qualitatively vary with averaging period (using instantaneous, monthly or daily data), though fine features and deviations such as σ reported for Figure 1 do depend on averaging.

[30] Results indicate that even monthly averages from the 26 level tropospheric model (CAM) do a reasonable job of reproducing the overall structure of the TTL. However, the high variability of the minimum lapse rate is best reproduced by diagnoses from instantaneous output. Ozone values vary with chemistry and model boundary conditions (emissions). As noted, the inclusion of emissions and tropospheric chemistry tend to increase the minimum ozone in the TTL (Figure 2). Otherwise, model results are similar. Except where noted, major features in one simulation are also seen in the others.

[31] Similar results are obtained for July (Table 2). As will be discussed below, the models and observations have a lower (~100 hPa) and warmer (~195 K) tropopause, with a similar level of LZH, LRM and O_3 minimum. CMAM and WACCM get the right seasonal gradients between maximum and minimum. In the case of CPT Temperatures, there are some 1–2 month shifts in maximum temperatures, which have also been noted by *Eyring et al.* [2006] for 100 hPa temperatures.

3.2. TTL Thermal Budget

[32] Figure 4 illustrates the thermal budget of the TTL in WACCM (Figure 4a) and WACCM and CMAM radiative heating rate profiles (Figures 4b and 4c). The thermal budget of the TTL is a balance between the total diabatic (DIABATIC) and dynamical (DYN) heating. The diabatic component is a combination of radiation (QNET) and total condensation (COND) terms. Parameterized gravity wave drag and diffusion (GW + D) are negligible contributions at TTL altitudes. The balance is similar to the results of *Boville et al.* [2006], where the "turbulent" term refers to condensation processes. Heating is negative from 275–150 hPa or

Table 2. As for Table 1 but for July

Model/Obs	CPT, K	CPT, hPa	LZH, hPa	LRM, hPa	$MinO_3$, hPa	$MinO_3$, ppbv
GPS	194.7	98		241		
RAOB/SHADOZ	194.9	99		249	294	35
WACCM L103 monthly	192.8	97	136	277	307	30
WACCM L103 daily	192.6	96	132	250	267	29
WACCM L103 instant	192.4	97		241	267	28
WACCM L66 monthly	192.2	90	139	266	353	29
CMAM instant	194.8	96	144	266	247	20
CAM L26	191.4	87	154	243	402	42

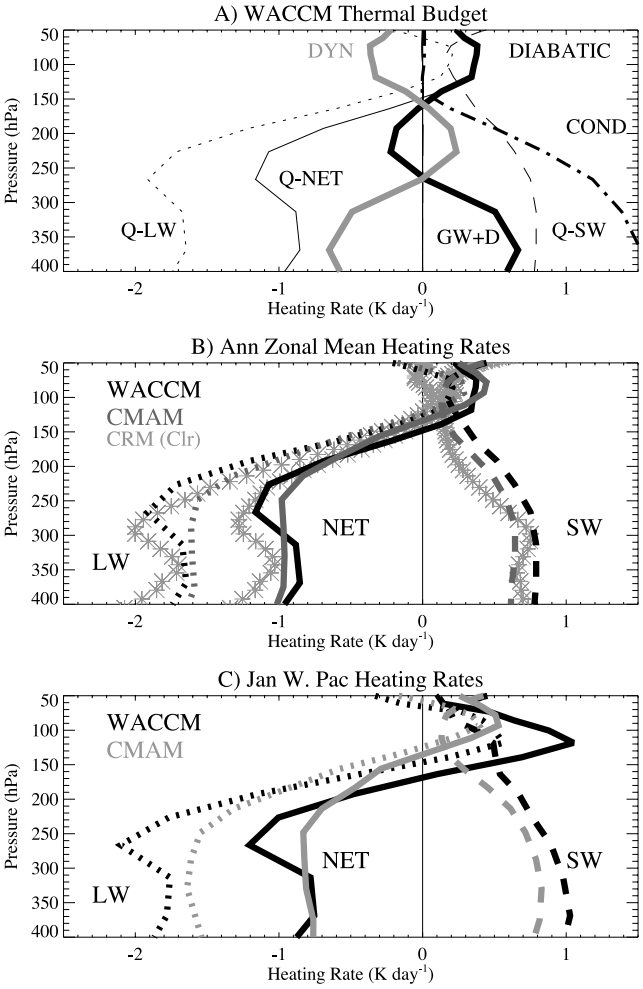

Figure 4. Tropical (20S–20N) thermal budget. (a) WACCM budget showing total diabatic heating (DIABATIC, thick solid black), dynamical heating (DYN, thick solid gray), long-wave (Q-LW, thin dotted), short-wave (Q-SW, thin dashed), and net (Q-NET, thin solid) radiative heating, total heating from condensation (COND, thick dot-dash), and heating from gravity waves and diffusion (GW + D thin dot dash, essentially zero). (b) Annual zonal mean radiative heating from WACCM (black) and CMAM (gray). Long wave (dotted), short wave (dashed), and net (solid). Offline clear sky heating calculation for September using observed temperature and trace gas profiles in light gray asterisks. (c) As for Figure 4b from WACCM and CMAM but for January western Pacific (105–180 lon) radiative heating.

so, due to a falloff in latent heat faster than the long-wave cooling from water vapor falls off. Above 150 hPa, there is virtually no latent heating, and the balance is between radiation and dynamics.

[33] The annual zonal mean tropical heating profiles (Figure 4b) in WACCM and CMAM are similar to each other and to an average clear sky profile calculated using a column radiation model observations over the Galapagos in September, taken from calculations by *Gettelman et al.* [2004] (light gray asterisks in Figure 4b). There are some differences between the clear sky and model all sky profiles due to clouds. In Figure 4b, the annual mean height of the level of zero heating is 148 hPa for WACCM, 134 hPa for CMAM (which are both all sky values) and 138 hPa for the Galapagos September profile (which is a clear sky value).

[34] There are some interesting differences between CMAM and WACCM. Figure 4c illustrates heating rate profiles for January over the western Pacific (105–180 longitude). WACCM has more long-wave cooling than CMAM from 200-70 hPa and more short-wave heating for a significantly larger net heating rate, and a lower level of zero heating. The results are robust across different model runs examined. Water vapor profiles show little difference between the two models, indicating that the difference is likely due to the difference in clouds (see below). Most of the differences occur in the TTL below the CPT.

3.3. Mean Structure of the TTL

[35] The basic structure of the TTL is well reproduced by the model simulations. The mean spatial structure is shown for January and July in Figure 5 using monthly data from CMAM. Similar plots from either of the WACCM simulations are qualitatively and quantitatively similar, except where noted below. Also plotted on the figure are stations for radiosonde or ozone data, with the location as a black asterisk, and the value indicated by a colored box.

[36] The cold point tropopause pressure (not shown) is nearly constant at 85 hPa. Cold point temperature (Figures 5a and 5b) has a similar structure to observations, with a minimum over the western Pacific and South America in January, as do the observations [*Highwood and Hoskins*, 1998]. In July (Figure 5), CPT is warmer, with a minimum off the equator associated with the Asian Monsoon. There is little spatial variation to the level of zero heating (not shown), which lies at about 140–150 hPa (Table 1 and Figure 4).

[37] The lapse rate minimum (LRM) pressure (Figures 5c and 5d) is lower (higher altitude) over the western Pacific, as is the level of the ozone minimum (Figures 5e and 5f), which has a similar structure but is slightly higher. The LRM pressure broadly follows convection and is at lower pressure in convective regions in the Southern Hemisphere in January (Figure 5d) and in the Northern Hemisphere in July (Figure 5d). This agrees well with the spatial pattern of observations of the LRM pressure, but it is opposite to the zonal mean behavior. There is less agreement with observations of the LRM outside of convective regions where the LRM is more distinct. The minimum ozone pressure is more concentrated in the western Pacific, but ozone minima occur in the summer subtropics in both January (Figure 5e) and July (Figure 5e). There is also broad agreement with SHADOZ ozone observations.

[38] The minimum mean Ozone value in the TTL (Figures 5g and 5h) is less than 20 ppbv in CMAM, centered over the western Pacific in a region of active convection, but the field is smooth due to the long lifetime of ozone. Consistent with Figure 2, CMAM has less ozone than WACCM, CAM or SHADOZ observations, in part due to the lack of NOx emissions from lightning. However, CMAM has approximately the right spatial gradients. Ozone minimum values are generally higher in July (Table 2).

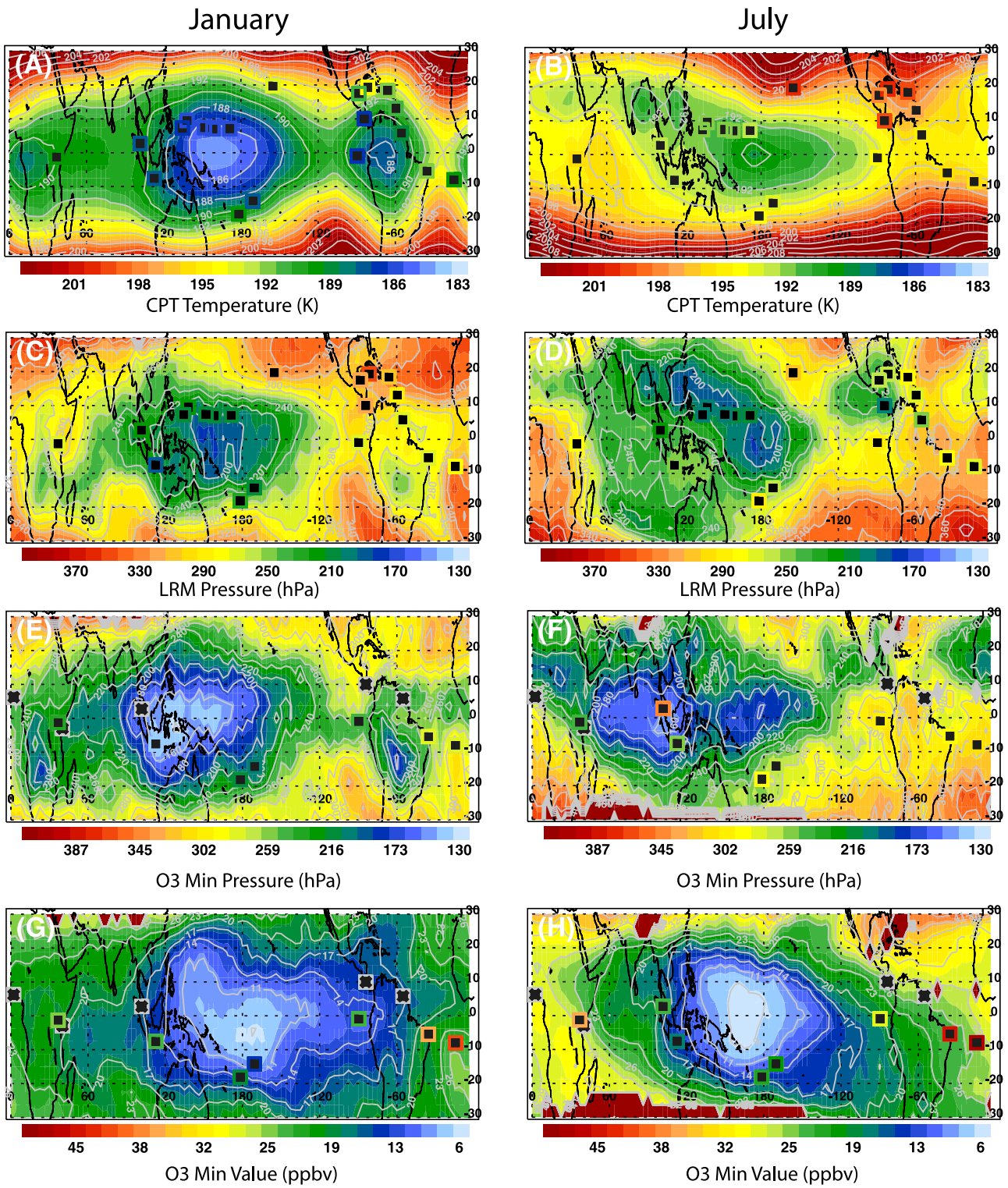

Figure 5. TTL maps of (a and b) Cold Point Tropopause temperature (in K), (c and d) pressure of the minimum lapse rate (in hPa), (e and f) pressure (hPa), and (g and h) value (ppbv) of the TTL ozone minimum, for (a, c, e, and g) January and (b, d, f, and h) July from CMAM. Asterisks indicate locations of observations from radiosondes and/or SHADOZ ozonesondes. Colored square indicates observed value. Undefined TTL ozone minima (minO3 pressure >500 hPa in more that 50% of the profiles) are marked by dark red colors (model) and black squares (sondes).

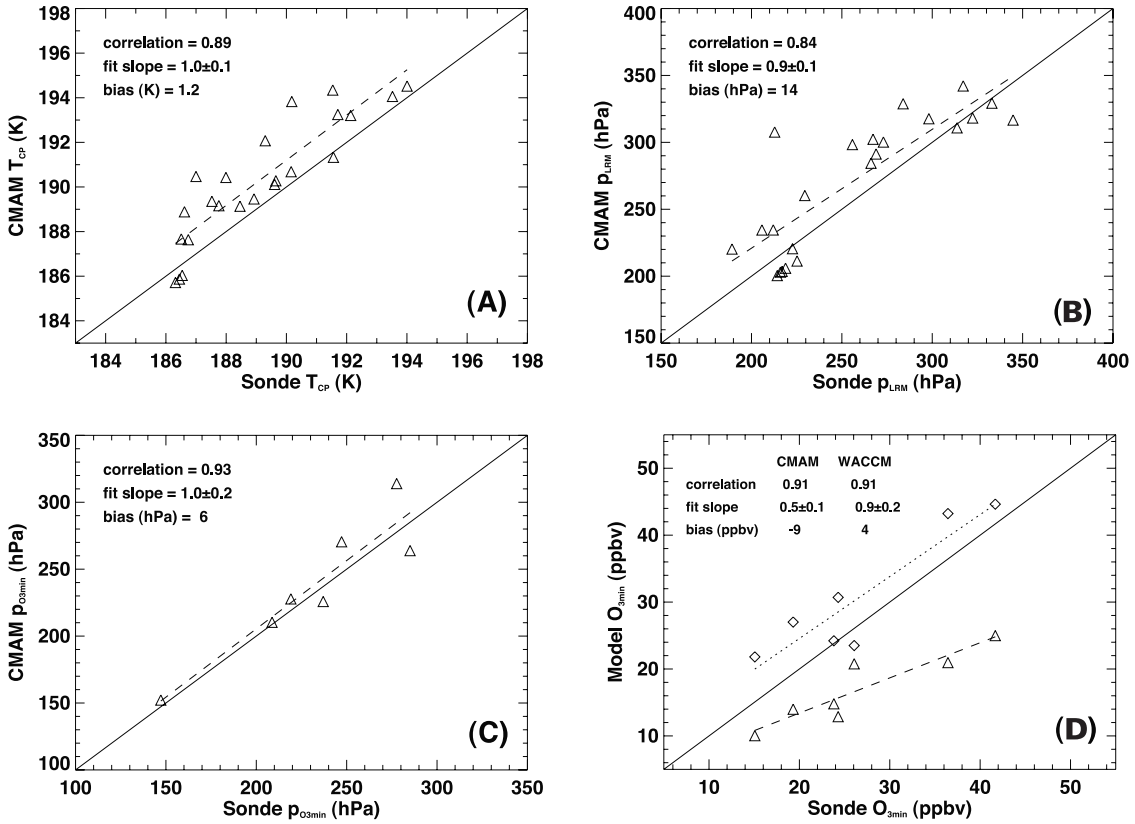

Figure 6. Scatterplots of CMAM January quantities against observations for (a) Cold Point Tropopause temperature, (b) pressure of the minimum lapse rate, (c) pressure, and (d) value of the TTL ozone minimum from CMAM. Locations correspond to Figure 5 as follows: (a) Figure 5a, (b) Figure 5c, (c) Figure 5e, and (d) Figure 5g. The fit slope and $\pm 1\sigma$ is a linear fit through the points (dashed line). The thin full line is the 1:1 line. Correlation is a simple correlation coefficient. WACCM data for ozone also shown in Figure 6d as diamonds and dotted line.

[39] Figure 5 for January and July also illustrates the seasonal evolution of the TTL. The structure of the tropopause is very different in the simulations in July (Figure 5b), but also resembles observations indicated in Figures 5a and 5b. There is a seasonal shift to the LZH (not shown), which is at higher pressure (lower altitude) in the summer hemisphere. This is consistent with enhanced TTL water vapor from convection in the summer hemisphere increasing TTL cooling and lowering the LZH level (higher pressure).

[40] The LRM pressure (Figures 5c and 5d) as noted, evolves with convection, and thus the LRM is at a lower pressure with greater convective activity in the summer hemisphere. The LRM has a persistent pressure minimum over the western Pacific. The minimum ozone level and value (Figures 5d and 5e) are similar between January and July. Minimum ozone pressure also seems to follow convection into the summer hemisphere. The sparse observations from SHADOZ show some of this feature, with disagreement around Indonesia, especially in July (Figure 5e), though variability in the observations appears to be larger than the total zonal range of the simulations in both January and July (Figures 5c and 5d).

[41] We have examined of the full annual cycle of the TTL diagnostics in Figure 5 (not shown). The annual cycle is consistent with the January & July extremes in Figure 5. The tropical mean CP Temperature is a maximum in boreal summer–fall and a minimum in boreal winter. CMAM, WACCM and CAM underestimate the amplitude of the annual cycle. There is little average seasonal variation in the LZH, but simply the alternating hemispheric pattern noted above. The minimum lapse rate also does not vary much in the tropical average over a year. The minimum value of ozone in the TTL has a semiannual cycle, with a slight increase in solstice seasons, and a minimum in equinox seasons, also seen by *Peters et al.* [2004].

[42] Figure 6 presents a different way of looking at the comparison between observations and CMAM. Scatterplots in Figure 6 illustrate the correspondence between CMAM and radio/ozone-sonde observations. The fit slope and $\pm 1\sigma$ is a linear fit through the points (dashed lines in Figure 6). The thin full line is the 1:1 line. The correlation is a simple correlation coefficient. For Cold Point Temperature (Figure 6a), LRM Pressure (Figure 6b) and Ozone minimum pressure (Figure 6c), there is a high correlation, and a slight positive bias to CMAM, indicating slightly warmer cold point temperatures, and slightly higher LRM and minO3 pressure (lower altitudes) than in the soundings. The minimum ozone value for CMAM is too low (Figure 6d), while WACCM has a much smaller positive bias. CMAM ozone does behave consistently (high corre-

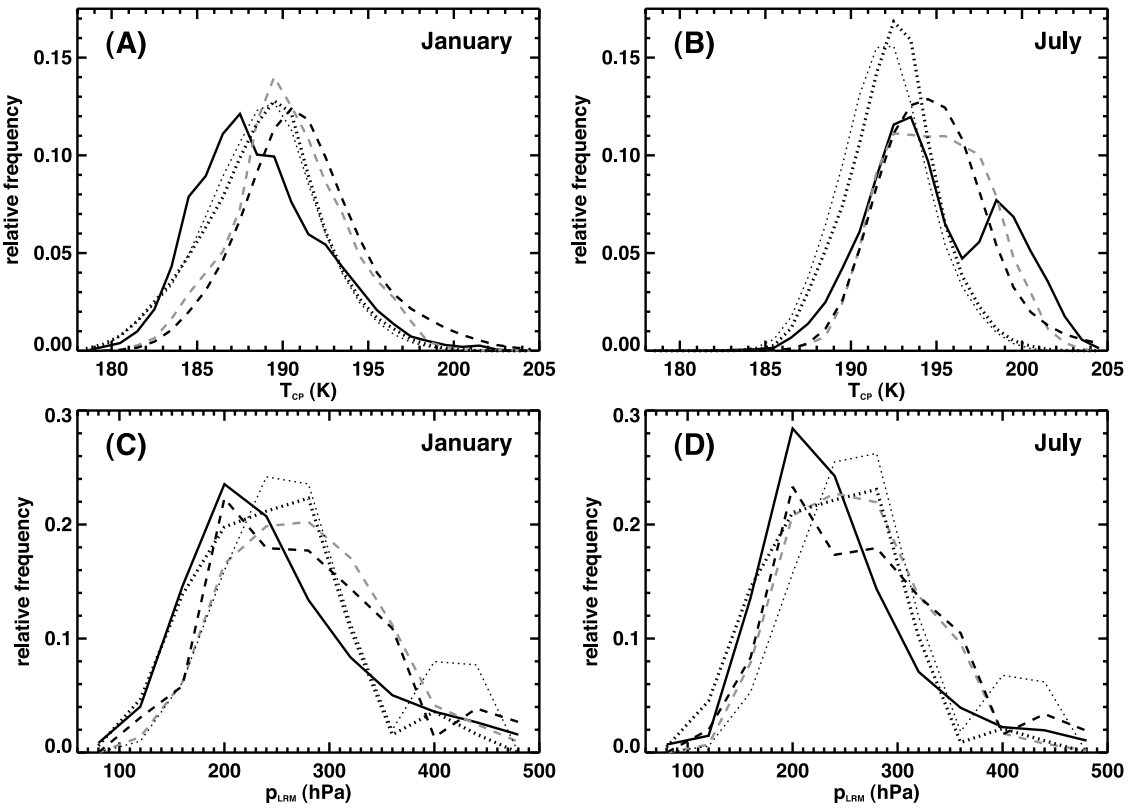

Figure 7. Probability Distribution Functions of TTL (20S–20N) (a and b) Cold Point Temperature and (c and d) the pressure of the Lapse Rate Minimum for (a and c) January and (b and d) July. Observations, solid; CMAM, dashed; WACCM, thick dotted; CAM, thin dotted. Gray dashed line is CMAM sampled only at sounding sites.

lation), but the low fit slope of 0.5 indicates a missing production process, most likely lightning production of NOx (see CMAM description).

[43] We have not discussed water vapor in the TTL, mostly because observations are very limited, and the variability of TTL water vapor (clear sky) does not seem to impact the TTL structure itself, even though water vapor is critical for cloud formation and for the stratosphere. However, as noted, the radiative effect of the mean water vapor distribution, which decays exponentially with height, is important for the radiative balance of the TTL. Also, we will discuss clouds (condensed water) further below. We do note that previous work [*Eyring et al.*, 2006; *Gettelman and Kinnison*, 2007] have shown that both CMAM and WACCM credibly simulate the seasonal evolution of water vapor at the top of the TTL and in the lower stratosphere. Both models are able to reproduce the observed vertically propagating annual cycle of stratospheric water vapor [*Mote et al.*, 1996]. This occurs because the models broadly reproduce the annual cycle of tropopause temperatures and structure (Figures 5a and 5b).

3.4. Variability

[44] Variability of cold point tropopause temperature in WACCM (L103) during January from instantaneous data is shown in Figure 1a. Minimum Cold Point Tropopause (CPT) temperatures are found in the western Pacific. The daily variations about the mean have a range of 10 K and the mean itself varies zonally from 184–195 K. Variability is less over the Atlantic. Agreement with GPS observations is remarkable. In the vertical, variability in temperature peaks near the CPT in observations [*Randel and Wu*, 2005], and this is also reproduced by WACCM (not shown).

[45] There is much broader variability associated with the minimum lapse rate level in Figure 1b. As noted, this level is generally higher in convective regions as the influence of convection tends to enhance the minimum lapse rate level. WACCM and GPS observations both show similarly wide scatter with the same standard deviation (70 hPa or 1.9 km), and a similar mean and zonal structure.

[46] The Probability Distribution Function (PDF) of CPT Temperature is shown in Figure 7 for January (Figure 7a) and July (Figure 7b) from CMAM (dashed), WACCM (thick dotted), CAM (thin dotted) and SHADOZ/RAOB observations (solid black). The gray line illustrates the CMAM distribution of CP Temperature sampled at the locations of the observations, indicating that due to sparse sampling, the observations are slightly colder than the tropical mean in January, and slightly warmer than the mean for July. Models are slightly warmer than observations for January and colder for July, which is partially a result of this sampling bias of the observations. Even so, models underrepresent the frequency of very cold temperatures, perhaps due to missing (1) small-scale waves or (2) overshooting convection. WACCM has less variation in July as

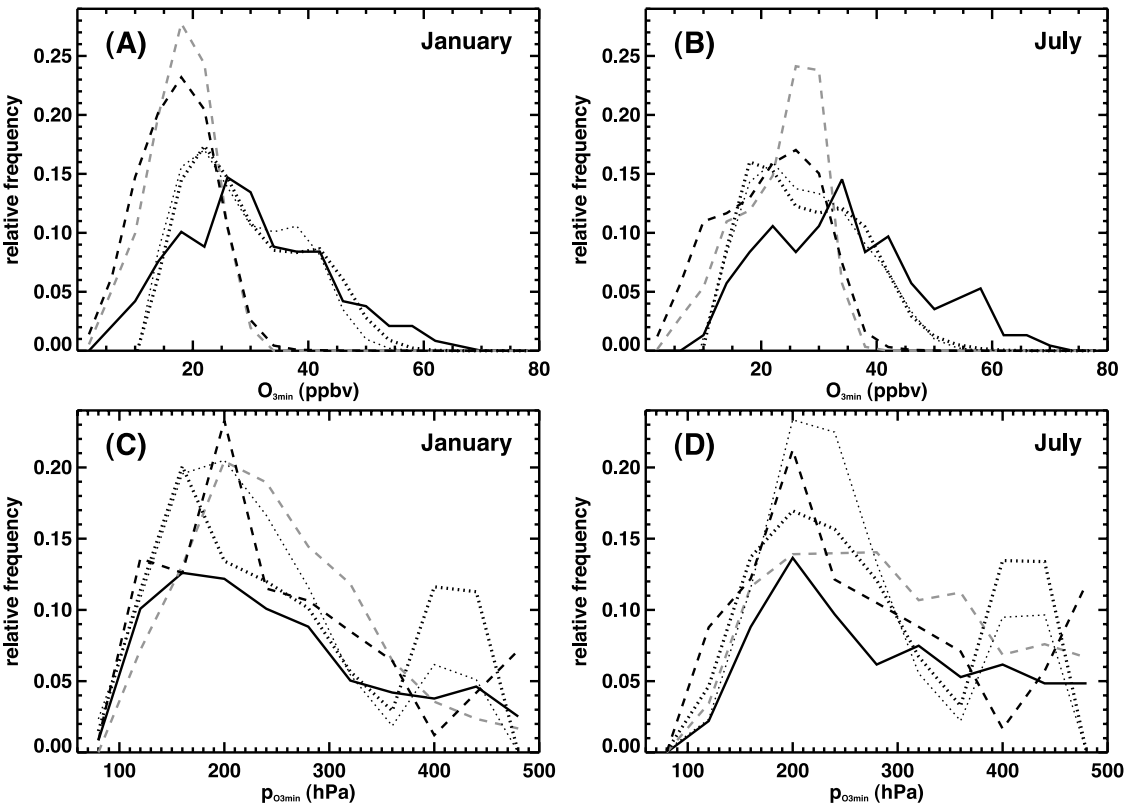

Figure 8. Probability Distribution Functions of TTL (20S–20N) (a and b) Minimum Ozone value and (c and d) pressure for (a and c) January and (b and d) July. Observations, solid; CMAM, dashed; WACCM, thick dotted; CAM, thin dotted. Gray dashed line is CMAM sampled only at sounding sites.

it does not fully capture the warm regions in the observations in July (Figure 7b), which come from the Caribbean stations in the observations (Figure 5b).

[47] PDFs of the pressure of the lapse rate minimum (LRM), representing the main convective outflow level, are shown in Figures 7c and 7d. A slight high pressure bias to the observations is indicated (by sampling CMAM at the observation points (gray line)). This indicates that the observed value might be at a slightly lower pressure (higher altitude) in the zonal mean. The models capture the variability of the LRM in Figure 7, with a high pressure (low altitude) bias. CAM has a mode near the base of the TTL that does not appear in the observations. Approximately 15% of model profiles do not have a minimum in lapse rate in the TTL ($p < 500$ hPa) and these points have not been included in the PDFs.

[48] A PDF of the ozone minimum is shown in Figure 8. Figures 8a and 8b show the minimum ozone value. As noted above, relative to SHADOZ ozone soundings, CMAM tends to have minima that are too low. CAM and WACCM minimum ozone tends to be slightly lower than observed minima with a peak near 25 ppbv, though the mean is higher (Tables 1 and 2). WACCM ozone is almost bi-modal (especially in July), with the low ozone values coming from the western Pacific, and higher values from the Atlantic region. WACCM and CAM do a decent job of representing the total distribution of the minimum ozone value. There is a broad distribution of this level of minimum ozone (Figures 8c and 8d) with the most probable value (peak of the PDF) around 200 hPa or less. Note that the distribution from CMAM sampled only at observed points (gray dashed line) is much broader than the distribution at all points. CAM and WACCM, with higher ozone, have a significant number of points with an ozone minimum at the upper edge of the pressure range, which also indicates an indistinct minimum (i.e., no O_3 minimum in the TTL, but a monotonic increase from the surface). This is common in non-convective regions (Figures 5e and 5f).

[49] Figure 9 shows the January monthly time-mean zonal and vertical temperature structure. Figure 9 can be compared to GPS observations of the TTL reported by *Randel et al.* [2003], their Figure 6. The tropical region (25S–25N) is slightly broader to include more GPS soundings in the average, but results are not highly sensitive to latitude. There are warm anomalies in convective regions (Indian and western Pacific Oceans) up to about 150 hPa (the level of zero heating), and then above these regions there is strong cooling, maximizing at the tropopause. The cold anomalies tilt eastward with height, and there are warm anomalies above cold anomalies in the troposphere in regions of descent in the Walker circulation. As discussed by *Randel et al.* [2003] and *Randel and Wu* [2005], this pattern is consistent with the large-scale equatorial wave response to latent heat release associated with convection. It maximizes near the base of the TTL at the level of main convective outflow (LRM, dashed line in Figure 9). The

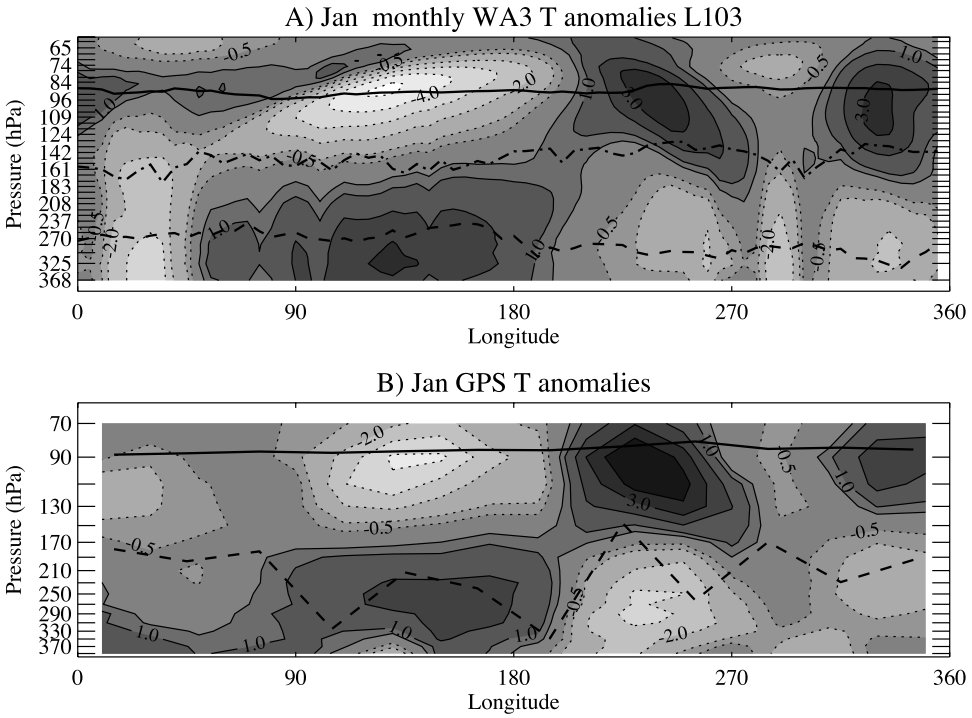

Figure 9. January tropical (25S–25N) temperature anomalies (deviations from the zonal mean) as a function of longitude and height from () WACCM L103 simulation and (b) GPS. Positive anomalies are solid; negative anomalies are dotted. Contour interval of ±1 K with ±0.5 K values added. Also shown is the meridional (25S–25N) average of the Cold Point Tropopause pressure (solid), the level of zero heating (dot-dash), and the level of the minimum lapse rate (dashed).

tilted structure is less evident in the GPS data than in WACCM, which may be due to insufficient sampling (as the tilt is seen in the GPS analysis by *Randel et al.* [2003]).

3.5. Clouds

[50] Perhaps the greatest uncertainty in simulating the TTL is the role of clouds. While most of the processes described above are either resolved or use well constrained parameterizations, because of the high space and time variability, condensation processes, and particularly convective processes, are not well simulated in global models. Thus while most of the previous results indicate agreement between models and observations in the TTL, clouds are one area where deficiencies (and differences between models) might be expected. In addition, tropical clouds, particularly thin cirrus and the tops of deep convection, are difficult to observe [*Sherwood et al.*, 2004] and thus existing observations of cloud structure in the TTL [*Gettelman et al.*, 2002b; *Liu and Zipser*, 2005] have large uncertainties.

[51] The vertical structure of total cloud in the TTL from WACCM is shown in Figure 10. Cloud fraction is mostly stratiform in the simulations, and this is particularly true at higher altitudes where stratiform clouds represent both cirrus clouds and anvil clouds. Note that in the WACCM simulations, convective clouds refer only to the cores of convective updrafts, calculated by the deep and shallow convective parameterizations in WACCM. Nonconvective clouds are calculated by a stratiform parameterization. Total clouds (or just "clouds") are the sum. Note that all cirrus clouds are stratiform clouds in the model. Clouds (mostly stratiform clouds) are found all the way up to the cold point and above. There is some cloudiness observed above the cold point (indicated as 84 hPa for January in Figure 10). There is a peak in cloudiness near 250 hPa, which represents the level of maximum convective outflow. There is significantly more cloudiness at the top of the TTL in January. Also shown in Figure 10 are cloud fraction from the Cloud-Aerosol Lidar and Infrared Pathfinder Satellite Observation (CALIPSO) [*Fu et al.*, 2007]. WACCM has a similar structure to CALIPSO observations, which indicate clouds up to 18 km (~70 hPa) with low frequency, and a peak in cloudiness in the TTL of 0.3 at 14 km (~140 hPa). The peak in CALIPSO data is higher than in WACCM (140 hPa versus 220 hPa). While both WACCM and CALIPSO have a mid-troposphere minimum, WACCM has higher cloud fractions in the lower troposphere and upper TTL, with higher cloud fractions from 300–150 hPa. The CALIPSO data in Figure 10 is referenced to log pressure altitude using a scale height of 7.0 km, so there is some uncertainty in exact pressure altitude.

[52] Figure 10 indicates that there are convective clouds up to the tropopause in January and July. We note that in WACCM convective cloud includes parameterized clouds from both a shallow and deep convection scheme, while CMAM does not have shallow convection. Convection in either scheme does not overshoot its level of neutral buoyancy. It is possible, particularly with high vertical resolution, to get some convective instability around the tropopause or on top of deep convection. This is observed in WACCM, but not in the atmosphere, and probably

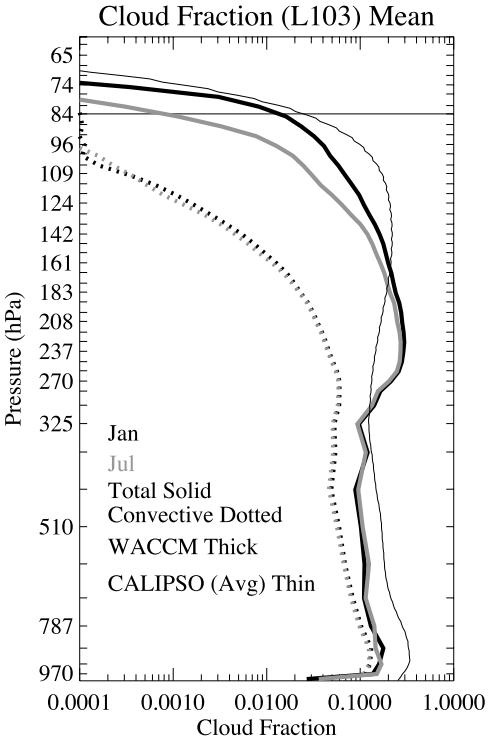

Figure 10. Tropical mean (20S–20N) cloud fraction from WACCM (L103) for January (black) and July (gray). Dotted lines are all cloud; solid lines are convective cloud only. Horizontal line is the January Cold Point Tropopause (84 hPa). Thin solid line is the June 2006 to February 2007 tropical mean cloud fraction from CALIPSO.

indicates a potential for continuous deep convection. Convective penetration is slightly higher if only the western Pacific is examined. CMAM (not shown) has a remarkably similar distribution of total cloudiness to Figure 10, with a peak at ~200 hPa and a rapid decrease to fractions of 0.001 at ~80 hPa, although convective cloud in CMAM never reaches the cold point, and stops well below the TTL, which causes differences in the radiative heat budget in cloudy regions (Figure 4). This does not seem to degrade CMAM's ability to reproduce the basic thermodynamic structure of the TTL.

[53] The locations of all cloud in the TTL and at the cold point are shown in Figure 11 for January (Figures 11a and 11b) and July (Figures 11c and 11d) in WACCM (L103). The peak frequency of cloud in the TTL is about 30% in January (Figure 11a). There is slightly more convection north of the equator in July (Figure 11c), associated with the Asian Monsoon and the Inter-Tropical Convergence Zone (ITCZ), but the tropical average (Figure 10) is lower in July than in January.

[54] The frequency of cloud at the cold point is several orders of magnitude lower than the peak frequency, and centered over the western Pacific in January (Figure 11b). There is less convection at the cold point in July (Figure 11d), and it is centered over the region of the Asian Monsoon. Note that cloud over Arabia in July in Figure 11d is a WACCM and CAM artifact and is not seen in observations [*Gettelman et al.*, 2002b]. These plots are qualitatively and quantitatively similar to those of *Gettelman et al.* [2002b], *Liu and Zipser* [2005], and *Fu et al.* [2007]. Plots of convective cloud at this level (not shown) indicate 2 orders of magnitude less cloud fraction, and may not be significant since convection is so infrequent at this level.

3.6. Water Vapor, Temperature, and Clouds

[55] Figure 12 shows a cross section of the western Pacific in January along the lines of Figure 6 of *Randel et al.* [2001]. Note that while the minimum temperatures are nearly symmetric around the equator, the water vapor minimum is shifted to the northern hemisphere, consistent with the mean circulation which rises in the summer (Southern) hemisphere and descends in the winter (Northern) hemisphere. This structure is also observed using satellite water vapor data by *Randel et al.* [2001], with slightly more hemispheric asymmetry in observed water vapor than in WACCM.

[56] Clouds (especially nonconvective cloud, thin black lines) are shifted into the northern hemisphere as well. Note that the model produces convective cloud maxima of equal strength on both sides of the equator, which is a known model bias, as the observations typically observe more convection in the summer hemisphere [*Gettelman et al.*, 2002b; *Randel et al.*, 2001]. Nonetheless, the relationships between temperature, clouds and water vapor discussed by *Randel et al.* [2001] are present in WACCM. Similar relationships are found in CMAM (not shown).

4. Discussion

[57] This analysis illustrates that models simulate most of the important features of the TTL, including both the mean and variability. Differences between models and observations are less than the variability or uncertainty in current observed data sets.

[58] There are not strong differences in the TTL between models used here. The two model families (WACCM and CMAM) have very different physical parameterizations for clouds, and different distributions of clouds in the TTL. CMAM does not have convection up to the cold point. If convection up to the cold point were important for either the large-scale mean or the large-scale variability of TTL temperatures then we would expect big differences between WACCM and CMAM. Both models capture the mean and the high frequency variability very well compared to RAOB and GPS observations.

[59] Even differences in radiative heating in regions of pervasive cloudiness such as the western Pacific do not seem to impact the mean TTL structure. Temperature and other diabatic processes are likely responding to make the overall diabatic heating similar in the models [*Boville et al.*, 2006]. So the TTL structure is not very different despite WACCM heating rates between the LZH and the cold point which are double those of CMAM (1 K day^{-1} for WACCM versus 0.5 K day^{-1} for CMAM). WACCM CPT Temperature is lower than CMAM, especially over the western Pacific in January, and the difference may be due to clouds and heating rates. Radiative heating is balanced by dynamic cooling due to upward motion, so the vertical velocities in the TTL will likely be different between the models, at least

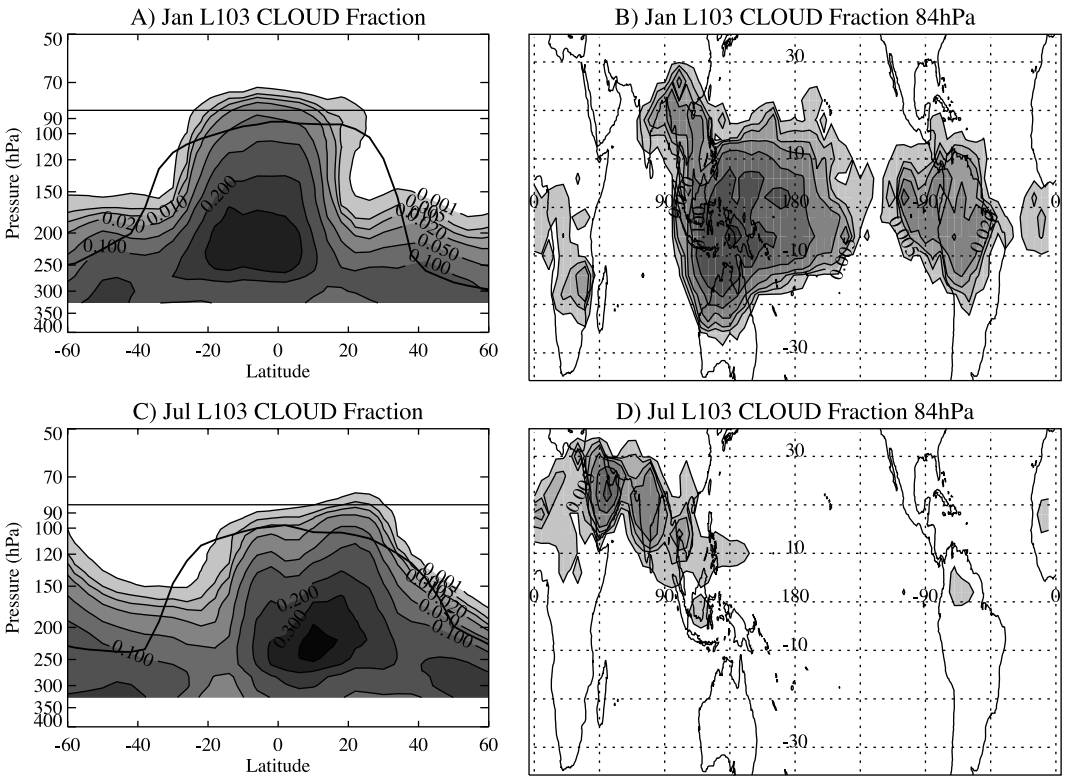

Figure 11. Cloud fraction from WACCM (L103) for (a and b) January and (c and d) July. Figures 11a and 11c show the zonal mean, with the thermal tropopause overplotted (thick line). The thin line is 85 hPa. Figures 11b and 11d show the locations of clouds at the level above the cold point (85 hPa). Contour intervals of 0.001, 0.005, 0.01, 0.02, 0.05, 0.1, 0.2, 0.3, and 0.4.

regionally. This means for example that WACCM will have larger vertical velocities over the western Pacific at the tropopause to balance the LW heating from thin clouds there, which do not exist in CMAM. These differences may not affect the temperatures, but do impact the processes responsible, and may affect the response to changes in clouds and radiation given anthropogenic forcing.

[60] The averaging period chosen, or sparse sampling of selected times does not seem to strongly affect these results. However, diagnostics for the base of the TTL (LRM, O3min) have large variability and may not be distinct outside of convective regions, so averaging may create some problems in diagnosing in particular the level of the ozone minimum. Model climatologies in the TTL do not seem to be very sensitive to vertical resolution, though there is some degradation of the CAM simulation at the top of the TTL, which may also be impacted by coarse representation of the stratosphere. High vertical resolution WACCM does simulate some of the finer-scale features (such as the stability jump above the tropopause) better than other

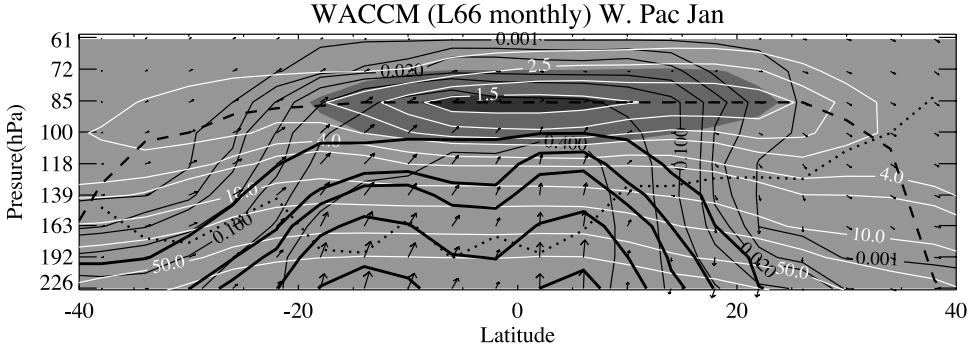

Figure 12. January cross section through the western Pacific (120–180E longitude) from 66 level WACCM. Temperature less than 185 K (dark) and 190 K (medium). Water vapor mixing ratio (ppmv) in white. Convective cloud frequency, thick solid black lines; all cloud frequency, thin solid black lines. Scaled wind vectors shown as arrows. Tropopause, dashed; level of zero heating, dotted.

models. Similar results are seen in a high resolution version of CMAM which is not included in this study. In total then, model simulations of the TTL are robust.

[61] On the basis of the limited set of existing observations, models do a reasonable job of reproducing the distribution of cloudiness in the TTL. What the models do well is to simulate two large-scale aspects of convection and cirrus clouds that are critical for the TTL. First, the overall integrated convective latent heating and its gross distribution, which are ultimately constrained by the global radiation balance of the tropics and the Hadley-Walker circulation. Second, bulk dehydration in stratiform (simulated cirrus) clouds which limits water vapor to values near the Clausius-Clapeyron limit. However, models are likely not treating convection properly within the TTL, and the detailed microphysics of cirrus clouds (for example, supersaturation over ice). These deficiencies do not appear to seriously compromise the simulated climatology of the TTL, and do not prevent the models from simulating the variability correctly at the scale of their resolution (200–400 km in the horizontal and 300–1000m in the vertical). Cloud microphysics and supersaturation may quantitatively influence water vapor concentrations, as both CMAM and WACCM have lower water vapor than observed [*Eyring et al.*, 2006] with temperature at or below observations (Tables 1 and 2), and do not include supersaturation. Thus including supersaturation may improve the simulations, as has been shown by *Gettelman and Kinnison* [2007]. Differences may also be due to differences in the Lagrangian cold point (Tables 1 and 2 represent Eulerian cold points), caused by transport [*Fueglistaler and Haynes*, 2005].

5. Conclusions

[62] These simulations indicate that the large-scale nonlocal response to convective heating (e.g., Figure 9) is most important for the TTL structure. It is not necessary to represent the details of convective or cirrus clouds above the level of maximum convective outflow to resolve the structure of the TTL. The simulations broadly are able to reproduce the main convective outflow level, and the distribution of convective and radiative heating in the tropics. Even significant regional biases in representations of convective patterns such as a "double ITCZ" or anomalous convection up to the tropopause (over Arabia seen in Figure 11d) do not seem to strongly affect the TTL structure or stratospheric water vapor. The models do reproduce the total precipitation, and thus total integrated latent heating, even if the timing and distribution are not correct.

[63] TTL structure is fundamentally determined by the radiative response to dynamical forcing. The radiative response is a combination of the reduction of water vapor with height, low temperatures and the presence of ozone and carbon dioxide, which both provide heating in the absence of other major absorbers. The radiative response is sensitive to clouds, but differences in radiative heating do not seem to strongly impact TTL structure. The TTL is also regulated by the stratospheric circulation above. The base of the TTL is determined by convection, and the evolution of the TTL and its structure are strongly influenced by the nonlocal effects of convective heating, which generate large-scale equatorial waves that affect transport and temperatures in the TTL. The radiative balance of the TTL is influenced by the distribution of clouds both below and at the tropopause.

[64] While the details of convective cloud processes may not be important for the climatology of the TTL, the details of cloud microphysics and convection might affect long term changes in the TTL, and may have a significant impact on the stratosphere. The balance of radiative and dynamical heating is regionally important in the simulations, and differs between WACCM and CMAM. The presence of thin cirrus near the tropopause regionally affects the thermal budget, which is coupled to the dynamical balance and may affect vertical motion. Thus changes to cirrus may impact TTL transport, and hence stratospheric water vapor and short lived species.

[65] Observations of clouds and convection in the TTL are still limited. Observations from CloudSat radar and CALIPSO lidar are starting to provide a much more detailed picture for comparison, and will allow us to better understand the details of TTL clouds and whether models are performing correctly, and for the right reasons.

[66] **Acknowledgments.** We thank the WACCM and CMAM teams for their hard work in model development, especially Byron Boville, Rolando Garcia, Doug Kinnison, and Stacy Walters (WACCM) and Stephen Beagley, David Plummer, John Scinocca, Kirill Semeniuk, and Knut von Salzen (CMAM). T.B. thanks James Anstey and Stephen Beagley for technical help. Useful comments on an earlier version of this manuscript were provided by Mijeong Park, Simone Tilmes, Ted Shepherd, David Plummer, and Norm MacFarlane. We also thank William Randel and Fei Wu for assistance with CHAMP GPS data and the SHADOZ and SPARC data centers for the availability of the sonde data. Thanks to Qiang Fu for access to CALIPSO data. This work is dedicated to the memory of Byron A. Boville, who had the foresight to push for the development of coupled chemistry climate models of the lower and middle atmosphere, without which this work would have been impossible. The National Center for Atmospheric Research is sponsored by the United States National Science Foundation. CMAM is supported by the Canadian Foundation for Climate and Atmospheric Sciences (CFCAS) and Environment Canada. T.B. acknowledges funding from CFCAS.

References

Atticks, M. G., and G. D. Robinson (1983), Some features of the structure of the tropical tropopause, *Q. J. R. Meteorol. Soc.*, *109*(460), 295–308.

Beagley, S. R., J. de Grandpré, J. Koshyk, N. A. McFarlane, and T. G. Shepherd (1997), Radiative-dynamical climatology of the first-generation Canadian Middle Atmosphere Model, *Atmos. Ocean*, *35*, 293–331.

Birner, T. (2006), Fine-scale structure of the extratropical tropopause region, *J. Geophys. Res.*, *111*, D04104, doi:10.1029/2005JD006301.

Birner, T., D. Sankey, and T. G. Shepherd (2006), The tropopause inversion layer in models and analyses, *Geophys. Res. Lett.*, *33*, L14804, doi:10.1029/2006GL026549.

Boville, B. A., P. J. Rasch, J. J. Hack, and J. R. McCaa (2006), Represenation of clouds and precipitation in the community atmosphere model version 3 (CAM3), *J. Clim.*, *19*(11), 2184–2198.

Brasseur, G. P., D. A. Hauglustaine, S. Walters, P. J. Rasch, J.-F. Muller, C. Granier, and X. X. Tie (1998), MOZART, a global chemical transport model for ozone and related chemical tracers: 1. Model description, *J. Geophys. Res.*, *103*(D21), 28,265–28,289.

Brewer, A. W. (1949), Evidence for a world circulation provided by the measurements of helium and water vapor distribution in the stratosphere, *Q. J. R. Meteorol. Soc.*, *75*, 351–363.

Collins, W. D., et al. (2006), The formulation and atmospheric simulation of the Community Atmosphere Model: CAM3, *J. Clim.*, *19*(11), 2122–2161.

Corti, T., B. P. Luo, Q. Fu, H. Vömel, and T. Peter (2006), The impact of cirrus clouds on tropical troposphere-to-stratosphere transport, *Atmos. Chem. Phys.*, *6*, 1725–1747.

de Grandpré, J., J. W. Sandilands, J. C. McConnell, S. R. Beagley, P. C. Croteau, and M. Y. Danilin (1997), Canadian Middle Atmosphere Model: Preliminary results from the chemical transport module, *Atmos. Ocean*, *35*, 385–431.

de Grandpré, J., S. R. Beagley, V. I. Fomichev, E. Griffioen, J. C. McConnell, A. S. Medvedev, and T. G. Shepherd (2000), Ozone climatology using interactive chemistry: Results from the Canadian Middle Atmosphere Model, *J. Geophys. Res.*, *105*, 26,475–26,491.

Dessler, A. E., S. P. Palm, W. D. Hart, and J. D. Spinhirne (2006), Tropopause-level thin cirrus coverage revealed by ICESat/Geoscience Laser Altimeter System, *J. Geophys. Res.*, *111*, D08203, doi:10.1029/2005JD006586.

Eyring, V., et al. (2006), Assessment of temperature, trace species, and ozone in chemistry-climate model simulations of the recent past, *J. Geophys. Res.*, *111*, D22308, doi:10.1029/2006JD007327.

Folkins, I., M. Loewenstein, J. Podolske, S. J. Oltmans, and M. Proffitt (1999), A barrier to vertical mixing at 14 km in the tropics: Evidence from ozonesondes and aircraft measurements, *J. Geophys. Res.*, *104*(D18), 22,095–22,102.

Folkins, I., C. Braun, A. M. Thompson, and J. Witte (2002), Tropical ozone as an indicator of deep convection, *J. Geophys. Res.*, *107*(D13), 4184, doi:10.1029/2001JD001178.

Folkins, I., P. Bernath, C. Boone, G. Lesins, N. Livesey, A. M. Thompson, K. Walker, and J. C. Witte (2006), Seasonal cycles of O3, CO, and convective outflow at the tropical tropopause, *Geophys. Res. Lett.*, *33*, L16802, doi:10.1029/2006GL026602.

Fu, Q., Y. Hu, and Q. Yang (2007), Identifying the top of the tropical tropopause layer from vertical mass flux analysis and CALIPSO lidar cloud observations, *Geophys. Res. Lett.*, *34*, L14813, doi:10.1029/2007GL030099.

Fueglistaler, S., and P. H. Haynes (2005), Control of interannual and longer-term variability of stratospheric water vapor, *J. Geophys. Res.*, *110*, D24108, doi:10.1029/2005JD006019.

Fujiwara, M., and M. Takahashi (2001), Role of the equatorial Kelvin wave in stratosphere-troposphere exchange in a general circulation model, *J. Geophys. Res.*, *106*(D19), 22,763–22,780.

Garcia, R. R., D. R. Marsh, D. E. Kinnison, B. A. Boville, and F. Sassi (2007), Simulation of secular trends in the middle atmosphere, 1950–2003, *J. Geophys. Res.*, *112*, D09301, doi:10.1029/2006JD007485.

Gettelman, A., and P. M. F. Forster (2002), A climatology of the tropical tropopause layer, *J. Meterol. Soc. Jpn.*, *80*(4B), 911–924.

Gettelman, A., and D. E. Kinnison (2007), The impact of supersaturation in a coupled model, *Atmos. Chem. Phys.*, *6*, 1629–1643.

Gettelman, A., W. J. Randel, S. Massie, F. Wu, W. G. Read, and J. M. Russell III (2001), El-Niño as a natural experiment for studying the tropical tropopause region, *J. Clim.*, *14*, 3375–3392.

Gettelman, A., W. J. Randel, F. Wu, and S. T. Massie (2002a), Transport of water vapor in the tropical tropopause layer, *Geophys. Res. Lett.*, *29*(1), 1009, doi:10.1029/2001GL013818.

Gettelman, A., M. L. Salby, and F. Sassi (2002b), Distribution and influence of convection in the tropical tropopause region, *J. Geophys. Res.*, *107*(D10), 4080, doi:10.1029/2001JD001048.

Gettelman, A., P. M. F. de Forster, M. Fujiwara, Q. Fu, H. Vmel, L. K. Gohar, C. Johanson, and M. Ammerman (2004), Radiation balance of the tropical tropopause layer, *J. Geophys. Res.*, *109*, D07103, doi:10.1029/2003JD004190.

Hajj, G. A., C. O. Ao, B. A. Iijima, D. Kuang, E. R. Kursinski, A. J. Mannucci, T. K. Meehan, L. J. Romans, M. de la Torre Juarez, and T. P. Yunck (2004), CHAMP and SAC-C atmospheric occultation results and intercomparisons, *J. Geophys. Res.*, *109*, D06109, doi:10.1029/2003JD003909.

Highwood, E. J., and B. J. Hoskins (1998), The tropical tropopause, *Q. J. R. Meteorol. Soc.*, *124*(549), 1579–1604.

Holton, J. R., P. H. Haynes, A. R. Douglass, R. B. Rood, and L. Pfister (1995), Stratosphere-troposphere exchange, *Rev. Geophys.*, *33*(4), 403–439.

Horowitz, L. W., et al. (2003), A global simulation of tropospheric ozone and related tracers: Description and evaluation of MOZART, version 2, *J. Geophys. Res.*, *108*(D24), 4784, doi:10.1029/2002JD002853.

Kinnison, D. E., et al. (2007), Sensitivity of chemical tracers to meteorological parameters in the MOZART-3 chemical transport model, *J. Geophys. Res.*, *112*, D20302, doi:10.1029/2006JD007879.

Kuang, Z., and C. S. Bretherton (2004), Convective influence on the heat balance of the tropical tropopause layer: A cloud-resolving model study, *J. Atmos. Sci.*, *61*(23), 2919–2927.

Küpper, C., J. Thuburn, G. C. Craig, and T. Birner (2004), Mass and water transport into the tropical stratosphere: A cloud-resolving simulation, *J. Geophys. Res.*, *109*, D10111, doi:10.1029/2004JD004541.

Liu, C., and E. J. Zipser (2005), Global distribution of convection penetrating the tropical tropopause, *J. Geophys. Res.*, *110*, D23104, doi:10.1029/2005JD006063.

Mote, P. W., et al. (1996), An atmospheric tape recorder: The imprint of tropical tropopause temperatures on stratospheric water vapor, *J. Geophys. Res.*, *101*(D2), 3989–4006.

Peters, W., M. C. Krol, J. P. F. Fortuin, H. M. Kelder, A. M. Thompson, C. R. Becker, J. Lelieveld, and P. J. Crutzen (2004), Tropospheric ozone over a tropical Atlantic station in the Northern Hemisphere: Paramaribo, Surinam (6°N, 55°W), *Tellus, Ser. B*, *56*, 21–34, doi:10.1111/j.1600-0889.2004.00083.x.

Potter, B. E., and J. R. Holton (1995), The role of monsoon convection in the dehydration of the lower tropical stratosphere, *J. Atmos. Sci.*, *52*(8), 1034–1050.

Randel, W. J., and F. Wu (2005), Kelvin wave variability near the equatorial tropopause observed in GPS radio occultation measurements, *J. Geophys. Res.*, *110*, D03102, doi:10.1029/2004JD005006.

Randel, W. J., A. Gettelman, F. Wu, J. M. Russell III, J. Zawodny, and S. Oltmans (2001), Seasonal variation of water vapor in the lower stratosphere observed in Halogen Occultation Experiment data, *J. Geophys. Res.*, *106*, 14,313–14,325.

Randel, W. J., F. Wu, and W. Rivera Ros (2003), Thermal variability of the tropical tropopause region derived from GPS/MET observations, *J. Geophys. Res.*, *108*(D1), 4024, doi:10.1029/2002JD002595.

Randel, W. J., F. Wu, H. Vmel, G. E. Nedoluha, and P. Forster (2006), Decreases in stratospheric water vapor after 2001: Links to changes in the tropical tropopause and the Brewer-Dobson circulation, *J. Geophys. Res.*, *111*, D12312, doi:10.1029/2005JD006744.

Robinson, F. J., and S. C. Sherwood (2006), Modeling the impact of convective entrainment on the tropical tropopause, *J. Atmos. Sci.*, *63*(3), 1013–1027.

Scinocca, J. F., and N. A. McFarlane (2004), The variability of modeled tropical precipitation, *J. Atmos. Sci.*, *61*, 1993–2015.

Sherwood, S. C., T. Horinouci, and H. A. Zeleznik (2003), Convective impact on temperatures observed near the tropical tropopause, *J. Atmos. Sci.*, *60*(16), 1847–1856.

Sherwood, S. C., J.-H. Chae, P. Minnis, and M. McGill (2004), Underestimation of deep convective cloud tops by thermal imagery, *Geophys. Res. Lett.*, *31*, L11102, doi:10.1029/2004GL019699.

Stephens, G. L. (2005), Cloud feedbacks in the climate system: A critical review, *J. Clim.*, *18*(2), 237–273.

Thompson, A. M., et al. (2003), Southern Hemisphere Additional Ozonesondes (SHADOZ) 1998–2000 tropical ozone climatology 1. Comparison with Total Ozone Mapping Spectrometer (TOMS) and ground-based measurements, *J. Geophys. Res.*, *108*(D2), 8238, doi:10.1029/2001JD000967.

Thuburn, J., and G. C. Craig (2002), On the temperature structure of the tropical substratosphere, *J. Geophys. Res.*, *107*(D2), 4017, doi:10.1029/2001JD000448.

Wickert, J., et al. (2001), Atmosphere sounding by GPS radio occultation: First results from CHAMP, *Geophys. Res. Lett.*, *28*(17), 3263–3266.

Zhang, G. J., and N. A. McFarlane (1995), Sensitivity of climate simulations to the parameterization of cumulus convection in the Canadian Climate Center general circulation model, *Atmos. Ocean*, *33*, 407–446.

T. Birner, Department of Physics, University of Toronto, 60 St. George Street, Toronto, ON, Canada M5S 1A7. (thomas@atmosp.physics.utoronto.ca)

A. Gettelman, Atmospheric Chemistry Division, National Center for Atmospheric Research, 1850 Table Mesa Drive, Boulder, CO 80305, USA. (andrew@ucar.edu)